COMMUNICATION

Differential adsorption of L- and D-lysine on achiral MFI zeolites as determined by synchrotron X-ray powder diffraction and thermogravimetric analysis

Tianxiang Chen,[a] Bolong Huang,[a] Sarah Day,[b] Chiu Chung Tang,[b] Shik Chi Edman Tsang,[c] Kwok-yin Wong,[a] Tsz Woon Benedict Lo[a,d*]

Abstract: We report the first crystallographic observation of stereospecific bindings of L- and D-lysine (Lys) in achiral ***MFI*** zeolites. The ***MFI*** structure has offered inherent geometric and internal confinement effects for the enantiomeric difference in L- and D-Lys adsorption. Notable difference over the sorption properties has been observed by circular dichroism (CD) spectroscopy and thermogravimetric analysis (TGA). Distinct L- and D-Lys adsorption behaviours on the H-ZSM-5 framework have been revealed by the Rietveld refinement of high-resolution synchrotron X-ray powder diffraction (SXRD) data and the density functional theory (DFT) calculation. Despite only demonstrated in L- and D-Lys over ***MFI*** zeolites at an atomistic resolution, the differential adsorption study sheds light towards the rational engineering of molecular interactions(s) with achiral microporous materials for chiral separation purposes.

Living organisms predominantly rely on the L-form enantiomer of amino acids[1,2], such as L-lysine (Lys) and L-arginine. The L- and D-enantiomers are only different in the optical property due to the presence of chiral carbon centre(s)[3]. There are, however, limited tools to characterise the stereochemistry of the biochemical and chemical species. To the best of our knowledge, to probe the chirality of amino acids, the only available technique is circular dichroism (CD) spectroscopy[4]. There is no other existing thermal, structural, spectroscopic or microscopic technique that can offer similar stereospecific investigation. CD relies on the observation of left-handed or right-handed circularly polarised light when the circular light interacts with a chiral centre.

As the production of non-100% enantiomeric excess (*ee*) is common in many chemical and pharmaceutical synthesis processes, reliable chiral separation materials are urgently required. Microporous materials, such as zeolites and metal-organic frameworks (MOFs), are one of the emerging sorbent materials for chiral separation *via* selection adsorption. It is because of their high internal surface area, high porosity, well-defined pore size and tuneable binding sites[5]. For example, chiral HMOF-1 was reported for Lys separation and achiral MIL-47 and MIL-53 for ibuprofen separation[5,6]. Based on the molecular simulation, the steric confinement effect exerted by the narrow porous structure of achiral MIL-47 and MIL-53 on the bulky ibuprofen molecules and leads to the stereospecific interactions. However, the synthesis of chiral microporous materials is challenging, which hinders their potential in broader commercial applications in chiral separation. Given the low-cost and high abundance of achiral zeolites and MOFs, it is critical to study how they can separate chiral molecules by achiral microporous materials. Based on DFT calculations, *van* Erp *et al.* have proposed the presence of 'chiral cells' in Al-rich ***MFI*** zeolites doped with Ca^{2+}[7]. Also, highly specific metal complexes with various amino acids and organic ligands have been heterogenised into host-zeolite matrices for catalysis applications; notable examples include zeolite-encapsulated metal-salen complexes[8] and zeolite-encapsulated amino acid–transition-metal complexes[9].

Our group has proven expertise in elucidating the surface interactions between gaseous adsorbate molecules and microporous materials by combining crystallographic and theoretical evidence. The slight-but-significant alteration of the scattering factors in diffraction data from *state-of-the-art* synchrotron X-ray facilities has enabled us to determine the atomic parameters of the adsorbate molecules about the framework. By further combining with periodic density functional theory (DFT) calculations, comprehensive kinetic and mechanistic information have been revealed[10,11]. The tertiary structures of the adsorbate-framework adducts demonstrate unique spatial and chemical properties, akin to the bio-enzymatic systems[12,13].

In this work, by taking advantages of the structural specificity of the zeolite ***MFI*** framework type and the molecular and stereo-specificities of L- and D-Lys, the sorption interactions between Lys and the zeolitic Brønsted acid sites (BASs) are revealed. By combining high-resolution synchrotron X-ray powder diffraction (SXRD) and DFT calculation, noticeably different adsorbate structures L- and D-Lys on H-ZSM-5 are revealed. Through *in-situ* SXRD and thermogravimetric analysis (TGA), the relationship between adsorption strengths and stereospecific adsorption geometries are established. This work undoubtedly illustrates that not only the intrinsic BAS strength but also the geometries for adsorption and stabilisation of the adsorbate species should be considered. The elucidation of the tertiary adsorbate structures can help to achieve high stereospecificity for biochemical and chemical processes.

Traditional Fourier-transform infra-red (FTIR) spectroscopy was used to probe the adsorption of amino acids on zeolites (see Figure S1 in SI). As seen in the normalised CD spectra

[a] T. X. Chen, B.L. Huang, K.Y. Wong, T.W. B. Lo
State Key Laboratory of Chemical Biology and Drug Discovery
Department of Applied Biology and Chemical Technology
The Hong Kong Polytechnic University, Hong Kong, China
E-mail: benedict.tw.lo@polyu.edu.hk
[c] S. Day. C. Tang
Diamond Light Source Ltd, Didcot OX11 0DE, UK
[d] S.C. E. Tsang
Wolfson Catalysis Centre, Department of Chemistry
University of Oxford
Oxford OX1 3QR, UK
[d] T.W. B. Lo
The Hong Kong Polytechnic University Shenzhen Research Institute
Shenzhen Hi-tech Industrial Park
Shenzhen 518000, China

Supporting information (SI) for this article is given via a link at the end of the document.

(*mdeg/mdeg*$_0$) in Figure 1 and Figures S2-S3, the H-ZSM-5 (SiO_2:Al_2O_3 = 46, 'H-ZSM-5(46)') adsorb L- and D-Lys at different extent, with k = -0.283(10) for L-Lys and k = -0.326(18) for D-Lys. It suggests that H-ZSM-5(46) can preferentially adsorb more D-Lys than L-Lys. Accordingly, TGA was employed to investigate the desorption behaviour from the zeolites. By adjusting the adsorption pH, the chemisorption of Lys onto the BAS via the α-carboxylate group[14]. From TGA, the sorption quantity and kinetics in L- and D-Lys from H-ZSM-5 are different, which agrees with the CD finding. The content of Lys adsorbed on H-ZSM-5 of L-Lys was measured as *ca*. 81 mg $g_{H\text{-}ZSM\text{-}5}^{-1}$ (0.55 mmol $g_{H\text{-}ZSM\text{-}5}^{-1}$) and of D-Lys 95 mg $g_{H\text{-}ZSM\text{-}5}^{-1}$ as (0.65 mmol $g_{H\text{-}ZSM\text{-}5}^{-1}$) at the adsorption pH of 2.2. The primary weight loss at lower temperatures (100 - 250 °C) can be ascribed to the desorption of Lys from the BASs. The weight loss below 100 °C can be ascribed to the removal of physisorbed species. However, the species removed from zeolites at higher temperatures could be the pyrolysis products of Lys[15]. For H-ZSM-5(46), the peak desorption temperature of L-Lys desorption is 11.3 °C higher than that of D-Lys; the difference is significant and far beyond standard experimental error. It suggests both the zeolitic structure and the framework-Al concentration can play pivotal roles in the differential adsorption of L- and D-Lys, which agrees with previous computational findings[7,16]. Besides the noticeable enantioselectivity as observed in high-Al H-ZSM-5(46), we also observed minor inconsistencies in the peak desorption temperatures in peak 2 in the low-Al H-ZSM-5(81, 300). As shown in the TGA of L- and D-Lys, most of the weight loss is observed at low temperature from the removal of physisorbed species. However, due to the minor and insignificant change in the TGA curves, it is hard to evaluate the difference with high certainty. From the experimental data, no clear pattern between the Al concentration (in H-ZSM-5) and the difference in TGA findings can be drawn. It is known that the Al position in zeolites is critically dependent on nature of the zeolite, precursors and synthesis conditions. Therefore, it infers that the differential adsorption property of Lys can be related to the crystallographic sitting of the Al in the H-ZSM-5 framework, which has also been demonstrated in a related computational study [7].

Similarly, the sorption properties at the adsorption pH of 1.0 have also been analysed (see Figure S4), and the peak desorption temperatures are summarised in Table S1 in SI. To probe the effect of zeolite framework type and acidity, H-MOR (***MOR***) and H-ZSM-5 (***MFI***) of different SiO_2:Al_2O_3 ratios were further studied (see Figure 1(c) and (d), Figure S5 and Table S2). The major pore system in H-ZSM-5 (***MFI*** framework type) possesses interconnecting straight and sinusoidal channels, whereas H-MOR only possesses straight channels (***MOR*** framework type) (Figure S6). The main peak desorption temperatures in the H-ZSM-5 samples were measured as *ca*. 150-170 °C, suggesting comparable BAS strength of the samples. The apparent activation energies for L- and D-Lys desorption from H-ZSM-5(46) have been approximated by the modified Arrhenius equation to be 16.69(2) and 18.96(2) kJ mol^{-1} respectively (see Figure S7 and Table S3 in SI), which fall in the diffusion control regime[17]. It suggests that the H-ZSM-5 structure may affect the desorption route of L- and D-Lys differently.

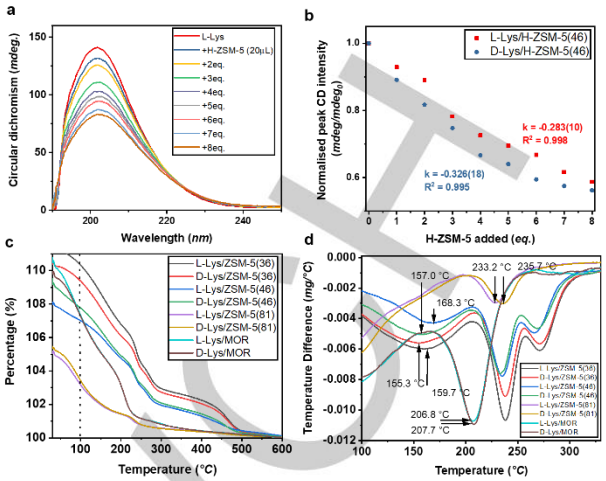

Figure 1. (**a**) CD spectra of L-Lys (10 mM) with the successive addition (20 uL) of H-ZSM-5 suspension (140 g L^{-1}), and the corresponding CD spectra of D-Lys are presented in Figure S2. Accumulation of three for averaging at each data point was taken to increase reliability. (**b**) The comparison of the normalised peak CD intensities (mdeg/mdeg$_0$) with respect to the H-ZSM-5 added. (**c**) TGA curves of L- and D-Lys desorption from H-ZSM-5 (SiO_2:Al_2O_3 = 36, 46, 81 and 300) and H-MOR zeolites (SiO_2:Al_2O_3 = 25) pre-adsorbed at pH 2.2, and (**d**) their corresponding differential curves. See details in Table S2.

Lys and Phe have different chemical and structural properties. The difference in the side chain R-group is: Lys has a lysyl side chain (straight chain), whereas Phe has a phenyl side chain (bulkier). Whilst H-MOR does not differentially adsorb L- and D-Lys, H-MOR illustrates notable enantioselectivity in the adsorption of L- and D-Phe (as shown in the CD and TGA measurements in Figure S3 and Table S2). In contrast to the proximate peak desorption temperatures of L- and D-Lys from H-MOR (*cf*. 206.8 °C and 207.7 °C), those of L- and D-Phe from H-MOR are noticeably different (*cf*. 206.8 °C and 201.7 °C). We postulate it can be caused by the confinement effect because of the bulkier Phe molecules. A more detailed discussion is described in the TGA section in the SI. Also, by comparing the peak desorption temperatures, the BAS strength (the ability to protonate incoming molecules) in H-ZSM-5 was found weaker than that of H-MOR. Previous computation findings have proposed that the BAS strength is highly dependent on the zeolite structure, and is governed by the SiO_2:Al_2O_3 ratio: the more acute is the ∠Si-O-Al, the stronger are of the BASs[18].

The Rietveld refinement of the SXRD data enables the direct visualisation of the adsorbate structures about the zeolitic framework. The synchrotron data were collected on Beamline I11 at Diamond Light Source (UK) and Beamline BL02B2 at SPring-8 (Japan). The X-ray energy of the incident beam was tuned to 15 keV with the calibrated λ = 0.824527(2) Å (Beamline I11) and 18 keV with the calibrated λ = 0.689556(2) Å) (BL02B2). The tuned energy for each beamline emits the optimum X-ray flux to achieve high contrast (signal-to-noise ratio) and high angular resolution.
In this communication, we will only focus on the adsorbate structures of L- and D-Lys on H-ZSM-5(46) as these two samples have the largest differences in TGA and CD measurements.

The SXRD patterns and the structural profiles are presented in Figure 2. The difference in the Bragg's peak intensities of the SXRD patterns of L- and D-Lys pre-adsorbed on H-ZSM-5 at pH 1.0 and 2.2 is subtle, but significant. It suggests that the adsorption behaviours of L- and D-Lys on H-ZSM-5 may affect the structural and atomic parameters. Supported by the good refinement fit (the small discrepancies in the grey difference profiles), and indicated by low-reliability factors (R_{wp}, R_{exp} and χ^2), the detailed structural parameters are presented in Table S4. At the adsorption pH of 1.0, the lattice volume is expanded by 0.33% upon L-Lys adsorption and by 0.28% upon D-Lys adsorption. Whereas, at the adsorption pH of 2.2, the lattice volume is expanded by 0.38% upon L-Lys adsorption and by 0.49% upon D-Lys adsorption. This agrees with the previous structural findings, where the adsorption of water by H-SAPO-34 increased the cell volume by *ca*. 0.5%[19]. From the *in-situ* SXRD measurements studying the temperature-programmed desorption behaviour, apparent differences in the desorption behaviours can be seen from the shape for the *in-situ* SXRD profiles in Figure 2.

The Rietveld refinements of the SXRD data collected on L- and D-Lys pre-adsorbed on H-ZSM-5 at pH 1.0 and 2.2 at 25 °C revealed two independent binding sites, I and II (Wyckoff letter of *4c* and *4c*), which are presented in Figure 3. It is in agreement with our previous adsorbate-framework studies of larger organic molecules. At the adsorption pH of 1.0, the total site occupancy factor (SOF, the sum of Sites I and II) of L-Lys in H-ZSM-5 was measured as 0.90(1) (94 mg $g_{H\text{-}ZSM\text{-}5}^{-1}$) and of D-Lys as 0.88(1) (92 mg $g_{H\text{-}ZSM\text{-}5}^{-1}$). Whereas, at the adsorption pH of 2.2, the total SOF of L-Lys in H-ZSM-5 was measured as 0.86(1) (90 mg $g_{H\text{-}ZSM\text{-}5}^{-1}$) and of D-Lys as 0.91(1) (95 mg $g_{H\text{-}ZSM\text{-}5}^{-1}$). Both agree with the TGA findings.

Site I is in the sinusoidal-straight cross-channel region and Site II is in the straight channel region. From the Rietveld refined structures, both L- and D-Lys exhibit an end-on interaction to the protonic BAS (δ+) *via* an oxygen of the *α*-carboxylate group (δ-). The variation in adsorption pH (pH 1.0 or 2.2) has a marginal effect over the adsorbate structures. However, the chirality of Lys plays a significant role in the adsorbate geometries on the H-ZSM-5 framework, as seen in the refined structures. Taking Site I as an example, the *α*-amino group in L-Lys is found to be located close to the opposite side of the *α*-carboxylate group of the 10-membered ring, whereas, for D-Lys, the *α*-amino and *α*-carboxylate groups interact with the same side of the 10-membered ring on H-ZSM-5. The side chain also exhibits different geometries, such as for D-Lys on H-ZSM-5, the tail of the side chain points downward, with the whole Lys molecule appears to be coiled up. This infers that the Site I of D-Lys may have higher potential energy with respect to the framework, whilst the Site I of L-Lys is less strained and expresses a more stable conformation. Similar crystallographic observations can also be seen in Site II where the 'tail' of the Lysyl R-group of L-Lys is directed to the centre of the sinusoidal channel exit, whereas that of D-Lys is located closer to the framework wall of the sinusoidal channel. From a molecular perspective, the non-Al adjacent $O_{framework}$ atoms are typically believed to be quite inert in forming interactions with incoming adsorbate species.

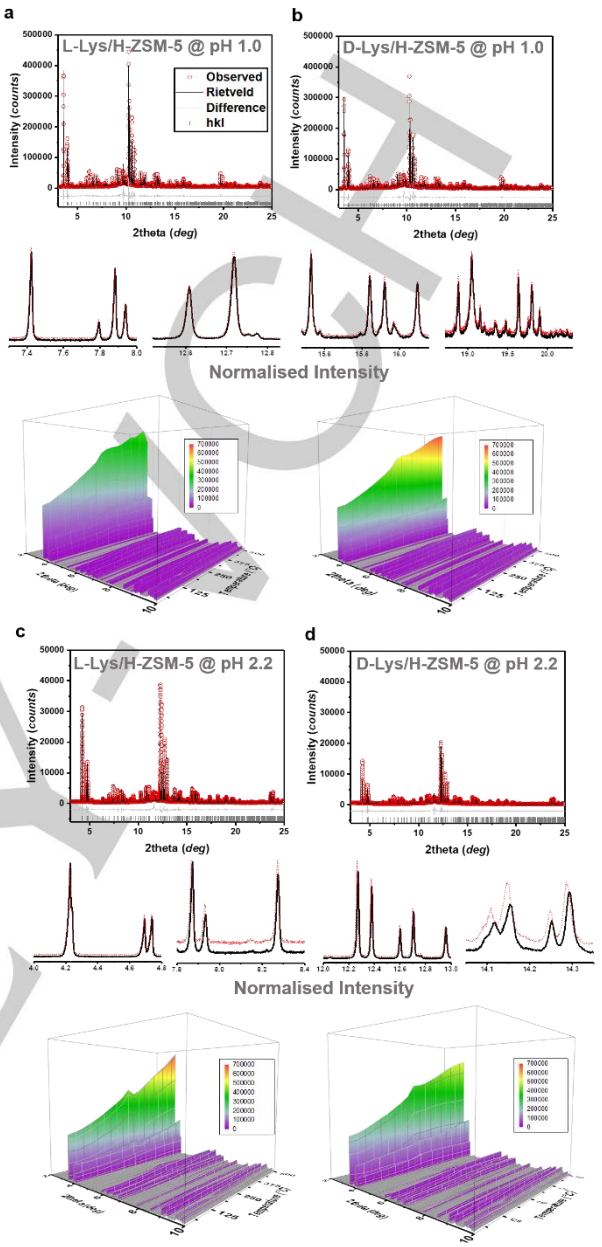

Figure 2. SXRD patterns and the structural profiles of H-ZSM-5 (SiO_2:Al_2O_3 = 46) pre-adsorbed with L- or D-Lys at (**a**, **b**) pH 1.0 (at 18 keV) or (**c**, **d**) pH 2.2 (at 15 keV) measured at 25 °C. The corresponding normalised (using the first Bragg's peak) SXRD patterns are shown, showing the subtle but significant difference in the peak intensity. The *in-situ* SXRD profiles (at 18 keV) of temperature-programmed desorption in nitrogen are also displayed.

To study the Lys-framework interactions at the atomistic resolution, the closest interatomic distance between the *α*-carboxylate and *α*-amino groups with the framework O atoms were analysed. Note that as H atoms cannot be directly located by this technique, the rigid framework O atoms are chosen as the crystallographic pointers in measuring the interatomic distances to represent the actual chemical acid-base information, i.e., $O_{framework}$-H…O_{Lys}. The interatomic distances are comparable to our previous reports that study other adsorbate molecules (namely, methanol[10,20], ammonia[12], pyridine[13], and furans[21–23]) on H-ZSM-5 and H-USY zeolites. It suggests the formation of

acid-base adducts between Lys and BASs. As seen in Figure 3, when L- and D-Lys are pre-adsorbed on H-ZSM-5(46) at pH 2.2, the closest interatomic distances observed at Site I are, for L-Lys: $O9_{LysI}$-$O18_{framework}$ = 2.47(3) Å and $N10_{LysI}$-$O15_{framework}$ = 3.03(3) Å, and for D-Lys: $O9_{LysI}$-$O18_{framework}$ = 3.02(3) Å and $N10_{LysI}$-$O21_{framework}$ = 2.74(3) Å, respectively. The crystallographic $O21_{framework}$ site is located on the opposite side of the 10-membered ring with respect to $O15_{framework}$. Whereas, for Site II, the closest interatomic distances observed are for L-Lys: $O8_{LysII}$-$O7_{framework}$ = 2.42(3) Å and $N10_{LysII}$-$O1_{framework}$ = 3.69(3) Å and for D-Lys: $O8_{LysII}$-$O7_{framework}$ = 2.40(3) Å and $N10_{LysII}$-$O5_{framework}$ = 3.37(3) Å. The closest interatomic distances for L- and D-Lys pre-adsorbed on H-ZSM-5 at pH 1.0 are comparable to those pre-adsorbed at pH 2.2. The refined adsorbate structures are verified with our DFT calculations (see Figure 4). Indeed, the adsorption mode and interatomic distances between L- and D-Lys and the H-ZSM-5 framework are comparable to each other.

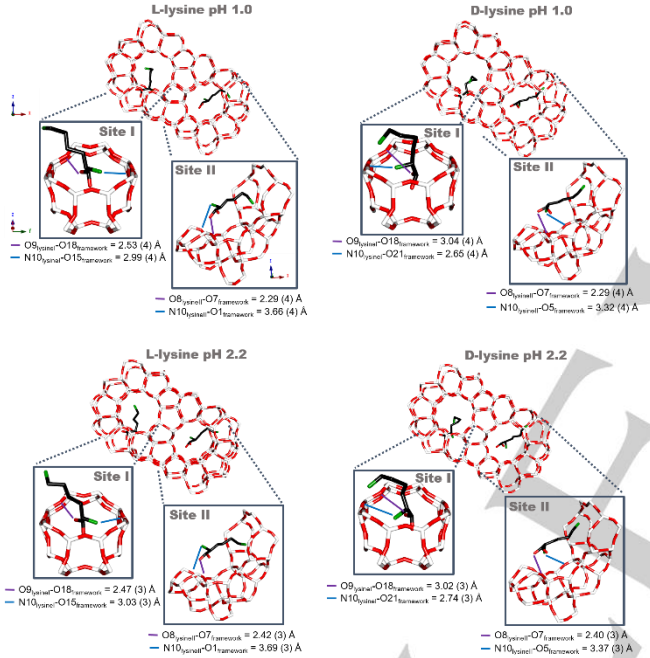

Figure 3. The Rietveld refined crystal structures of L- and D-Lys pre-adsorbed on H-ZSM-5 (SiO_2:Al_2O_3 = 46) at pH 1.0 and 2.2. Two adsorption sites are observed. The closest interatomic distances between the framework and L- and D-Lys are measured. For clarity, the mirror symmetry of the Lys adsorbates is disregarded. Ball-and-stick model: white = Si, red = O, black = C, and green = N. No hydrogens are plotted for clarity. See Rietveld refinement details in the experimental section and the Rietveld refinement verification in Table S5. See the atomic parameters in Table S6.

As reported in our previous works, Site I of the H-ZSM-5 sample was determined to be the strongest adsorption site by in-situ SXRD measurements[12,13]. We have therefore employed DFT calculation to study the adsorbate binding structures and binding strengths at Site I. Our theoretical results derived from the DFT calculations within the CASTEP of the L- and D-Lys in H-ZSM-5 zeolite support the above experimental observations packages (see computational details in SI/method)[24–26]. The DFT calculations investigated the binding behaviours of both L- and D-Lys on H-ZSM-5 (Al at T6 crystallographic site[12,13]). The relaxed structure of the binding are behaviours are shown in Figure 4 (a)-(b), which is consistent with the Rietveld refined crystal structures in Figure 3. The O…O and N…O interatomic distances are in the range between 2.5 – 3.1 Å, supporting the refinement results. The corresponding electron density plots show a slight difference (see Figure 4 (c) and (d)). The binding energy of L-Lys on H-ZSM-5 is substantially reduced to 0.17 eV at 0 K, whereas D-Lys has a much higher barrier of 4.71 eV at 0 K to achieve stable binding (see Figure 4(e)). The binding preference is also reflected by the projected partial density of states (PDOS). The overall electronic distribution of the local region of H-ZSM-5 has been modified by the binding of L-Lys, and noticeably shifted the valence bands. By further comparing the PDOS (see Figure 4(f)), the H-ZSM-5 framework can better stabilise L-Lys on the internal surface. From the DFT calculated difference in adsorption binding energies, the differential adsorption of Lys as observed can be accordingly explained. Consistent with the TGA and CD findings, L-Lys is more preferentially adsorbed by the H-ZSM-5 samples. the BAS and the ***MFI*** framework make the channel exit at the intersection physically different from each other and renders an active chiral environment to offer enantiospecific location adsorption geometries for L- and D-Lys.

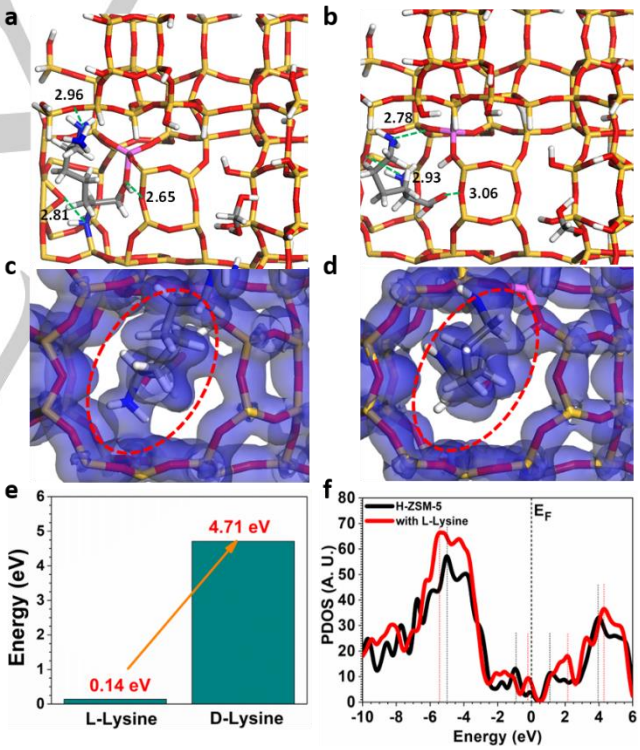

Figure 4. Relaxed binding structures by DFT calculations of (**a**) L-Lys and (**b**) D-Lys on H-ZSM-5. The corresponding electron density plot of (**c**) L-Lys and (**d**) D-Lys binding on H-ZSM-5. (**e**) Overall binding energy comparison at 0 K and (**f**) PDOS comparison.

In summary, the interactions between chiral L- and D-Lys molecules and the achiral microporous surface of H-ZSM-5 have been elucidated at an atomistic resolution. ***MFI*** and ***MOR*** with specific framework Al distribution show notably different enantioselective properties on straight-chain Lys and bulkier Phe. In agreement with previous computational reports, achiral zeolite framework can provide unique local adsorption geometry, which

may consequently offer enantioselectivity. This combined structural-computational analysis can be transferable to investigate the stereochemistry in related microporous materials, which can also offer practical insights into the rational design of achiral solid-state materials for chiral separation.

Acknowledgements

We thank the Hong Kong Research Grants Council (PolyU 253009/18P) and the National Natural Science Foundation of China (21902139) for financial support. We thank SPring-8 (2018B1081) and Diamond (NT23230-1) for the provision of beamtime, and UMF, UCEA and ULS of HKPU for the support in material characterisation.

Keywords: chirality • microporous materials• structural elucidation• X-ray diffraction

[1] G. Rikken, E. Raupach, *Nature* **2000**, *405*, 932.
[2] M. Yamanaka, Y. Miyoshi, H. Ohide, K. Hamase, R. Konno, *Amino Acids* **2012**, *43*, 1811–1821.
[3] M. M. Coles, D. L. Andrews, *Phys. Rev. A* **2012**, *85*, 63810.
[4] J. Yeom, B. Yeom, H. Chan, K. W. Smith, S. Dominguez-Medina, J. H. Bahng, G. Zhao, W.-S. Chang, S.-J. Chang, A. Chuvilin, *Nat. Mater.* **2015**, *14*, 66.
[5] L. Ma, J. M. Falkowski, C. Abney, W. Lin, *Nat. Chem.* **2010**, *2*, 838.
[6] R. Bueno-Perez, A. Martin-Calvo, P. Gómez-Álvarez, J. J. Gutiérrez-Sevillano, P. J. Merkling, T. J. H. Vlugt, T. S. van Erp, D. Dubbeldam, S. Calero, *Chem. Commun.* **2014**, *50*, 10849–10852.
[7] T. S. van Erp, T. P. Caremans, D. Dubbeldam, A. Martin-Calvo, S. Calero, J. A. Martens, *Angew. Chemie Int. Ed.* **2010**, *49*, 3010–3013.
[8] F. Li, D. Hu, Y. Yuan, B. Luo, Y. Song, S. Xiao, G. Chen, Y. Fang, F. Lu, *Mol. Catal.* **2018**, *452*, 75–82.
[9] D. J. Xuereb, J. Dzierzak, R. Raja, *Catal. Today* **2012**, *198*, 19–34.
[10] B. T. W. Lo, L. Ye, G. G. Z. Chang, K. Purchase, S. Day, C. C. Tang, D. Mei, S. C. E. Tsang, *Appl. Catal. B Environ.* **2018**, *237*, 245–250.
[11] B. T. W. Lo, L. Ye, C. A. Murray, C. C. Tang, D. Mei, S. C. E. Tsang, *J. Catal.* **2018**, *365*, 145–152.
[12] L. Ye, B. T. W. Lo, J. Qu, I. Wilkinson, T. Hughes, C. A. Murray, C. C. Tang, S. C. E. Tsang, *Chem. Commun.* **2016**, *52*, 3422–3425.
[13] B. T. W. Lo, L. Ye, J. Qu, J. Sun, J. Zheng, D. Kong, C. A. Murray, C. C. Tang, S. C. E. Tsang, *Angew. Chemie - Int. Ed.* **2016**, *55*, 5981–5984.
[14] R. Chatterjee, E. Welty, R. Y. Walder, S. L. Pruitt, P. H. Rogers, A. Arnone, J. A. Walder, *J. Biol. Chem.* **1986**, *261*, 9929–9937.
[15] J. R. Vallentyne, *Geochim. Cosmochim. Acta* **1968**, *32*, 1353–1356.
[16] A. Martin-Calvo, S. Calero, J. A. Martens, T. S. van Erp, *J. Phys. Chem. C* **2013**, *117*, 1524–1530.
[17] S. R. Logan, *Trans. Faraday Soc.* **1967**, *63*, 1712–1719.
[18] K. Suzuki, Y. Aoyagi, N. Katada, M. Choi, R. Ryoo, M. Niwa, *Catal. Today* **2008**, *132*, 38–45.
[19] D. S. Wragg, R. E. Johnsen, P. Norby, H. Fjellvag, *Microporous Mesoporous Mater.* **2010**, *134*, 210–215.
[20] B. T. W. Lo, L. Ye, C. A. Murray, C. C. Tang, D. Mei, S. C. E. Tsang, *J. Catal.* **2018**, *365*, 145–152.
[21] L. Ye, I. F. Teixeira, B. T. W. Lo, P. Zhao, S. C. Edman Tsang, E. Tsang, *Chem. Commun.* **2017**, *53*, 9725–9728.
[22] I. F. Teixeira, B. T. W. Lo, P. Kostetskyy, M. Stamatakis, L. Ye, C. C. Tang, G. Mpourmpakis, S. C. E. Tsang, *Angew. Chemie Int. Ed.* **2016**, *55*, 13061–13066.
[23] I. F. Teixeira, B. T. W. Lo, P. Kostetskyy, L. Ye, C. C. Tang, G. Mpourmpakis, S. C. E. Tsang, *ACS Catal.* **2018**, 1843–1850.
[24] Q. Sun, N. Wang, Q. Bing, R. Si, J. Liu, R. Bai, P. Zhang, M. Jia, J. Yu, *Chem* **2017**, *3*, 477–493.
[25] Y. Li, J. Yu, *Chem. Rev.* **2014**, *114*, 7268–7316.
[26] M. Fischer, R. G. Bell, *J. Phys. Chem. C* **2013**, *117*, 24446–24454.

Entry for the Table of Contents (Please choose one layout)

COMMUNICATION

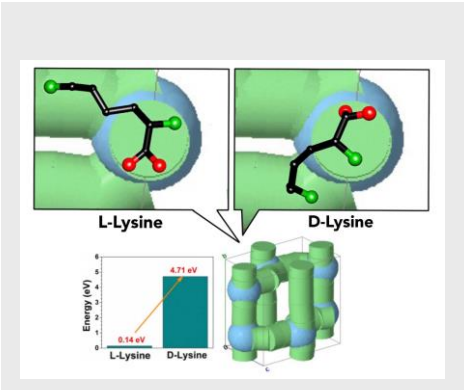

*Tianxiang Chen, Bolong Huang, Sarah Day, Chiu Chung Tang , Shik Chi Edman Tsang, Kwok-yin Wong, Tsz Woon Benedict Lo**

Page No. – Page No.

Differential adsorption of L- and D-Lys on achiral MFI zeolites as determined by synchrotron X-ray powder diffraction and thermogravimetric analysis

Differential adsorption behaviour of L- and D-Lys over H-ZSM-5 has been observed experimentally by circular dichroism (CD) spectroscopy and thermogravimetric analyses (TGA). The fundamental reason is explained by the structural study based on the Rietveld refinement of the high-resolution synchrotron X-ray powder diffraction (SXRD) data and the density functional theory (DFT) calculation.